UCRL 5596

MASTER

UNIVERSITY OF CALIFORNIA

Ernest O. Lawrence

Radiation Laboratory

LIVERMORE SITE

DISCLAIMER

This report was prepared as an account of work sponsored by an agency of the United States Government. Neither the United States Government nor any agency Thereof, nor any of their employees, makes any warranty, express or implied, or assumes any legal liability or responsibility for the accuracy, completeness, or usefulness of any information, apparatus, product, or process disclosed, or represents that its use would not infringe privately owned rights. Reference herein to any specific commercial product, process, or service by trade name, trademark, manufacturer, or otherwise does not necessarily constitute or imply its endorsement, recommendation, or favoring by the United States Government or any agency thereof. The views and opinions of authors expressed herein do not necessarily state or reflect those of the United States Government or any agency thereof.

DISCLAIMER

Portions of this document may be illegible in electronic image products. Images are produced from the best available original document.

UCRL-5596

UNIVERSITY OF CALIFORNIA
Lawrence Radiation Laboratory
Livermore, California

Contract No. W-7405-eng-48

GAMMA RAYS FROM THE INTERACTION OF 14-Mev NEUTRONS WITH BERYLLIUM

J. Benveniste, A.C. Mitchell,
C.D. Schrader and J.H. Zenger

June 9, 1959

Printed for the U.S. Atomic Energy Commission

GAMMA RAYS FROM THE INTERACTION OF 14-Mev NEUTRONS WITH BERYLLIUM

J. Benveniste, A.C. Mitchell,
C.D. Schrader and J.H. Zenger

Lawrence Radiation Laboratory, University of California
Livermore, California

ABSTRACT

The cross section for the $Be^{9}(n, t')Li^{7*} \rightarrow Li^{7} + \gamma$ (0.477 Mev) reaction has been measured in the vicinity of 14 Mev by detecting the gamma-rays at scattering angles from 30 to 150 degrees. A time-of-flight technique was used to distinguish the gamma-rays from the high neutron background. The cross section drops from 20 mb at 13.6 Mev to 10 mb at 14.1 Mev and then rises to 30 mb at 14.7 Mev.

INTRODUCTION

A time-of-flight technique has been employed for the study of gamma rays originating in the interaction of 14-Mev neutrons with various nuclei. Although we have used this technique to measure the spectral lines and angular distributions from several elements (some of this work was mentioned in a preliminary paper[1]), the present full report will be confined to our observations on Be because of (a) the simplicity of the gamma-ray spectrum, and (b) the relative ease of making calculations necessary to correct for contributions due to secondary processes. Previous efforts by others to detect gamma rays in the presence of high, continuous neutron fluxes have been hampered due to the discouragingly low signal-to-noise ratio. Through the use of short neutron bursts and a suitable flight path between the scatterer and the detector, however, the difference in time of arrival between the gamma rays and any other reaction products can be easily distinguished. The system described below exploits this fact to reduce the background substantially. In brief, the spectrometer is gated on only during those intervals in which gamma rays are being received at the detector.

DESCRIPTION OF EXPERIMENT

The accelerator used was a 500-kev Cockcroft-Walton machine. The deuteron beam emanating from the rf ion source was accelerated, then swept and bunched (see Appendix I) into pulses of 3-μsec duration at a repetition rate of 5 Mc/sec, which finally impinged on a titanium-tritium target producing 14-Mev neutrons through the reaction

$$D + T \rightarrow n + He^4.$$

The reaction was monitored by counting the alpha particles in a gas proportional counter mounted on the beam pipe in such a position that it received alphas which were emitted at an angle of 174° with respect to the deuteron beam.

The gamma rays resulting from the interaction of the neutrons in the scattering ring (see Fig. 1) placed near the tritium target were detected by a scintillation counter which was shielded on the sides by a 4-in.-thick cylinder of lead. In order to eliminate changes in pulse-height output due to temperature changes in the scintillator and photomultiplier, the entire detector and lead shield were maintained at a temperature of 15°C by cooling water from a portable refrigeration unit. An 18-in.-long copper slug suspended between the target and the detector attenuated the direct flux of neutrons reaching the detector by a factor of 30.

The 4050-g, 5-cm by 5-cm cross-section, 33-cm-o.d. Be ring was suspended from a cart on a track that was elevated high enough above the target so that no unshielded path existed between the track and the detector. By remote control the ring could be moved so that the angle θ, between the incident neutron and the detected gamma ray, could be varied continuously between 30° and 150°.

A block diagram of the detector-analyzer system is shown in Fig. 2. The detector proper consisted of a 2.06-in.-long by 1.78-in.-diam. NaI(Tl) cylinder mounted on a 6810A RCA photomultiplier tube. Each signal from the photomultiplier was split into a fast signal (taken from the anode and clipped to a width of 50 millimicroseconds) used in the gating system, and a slow signal (taken from the 9th dynode) which was analyzed. In order to isolate the fast signal from the slow, two high-voltage supplies were used.

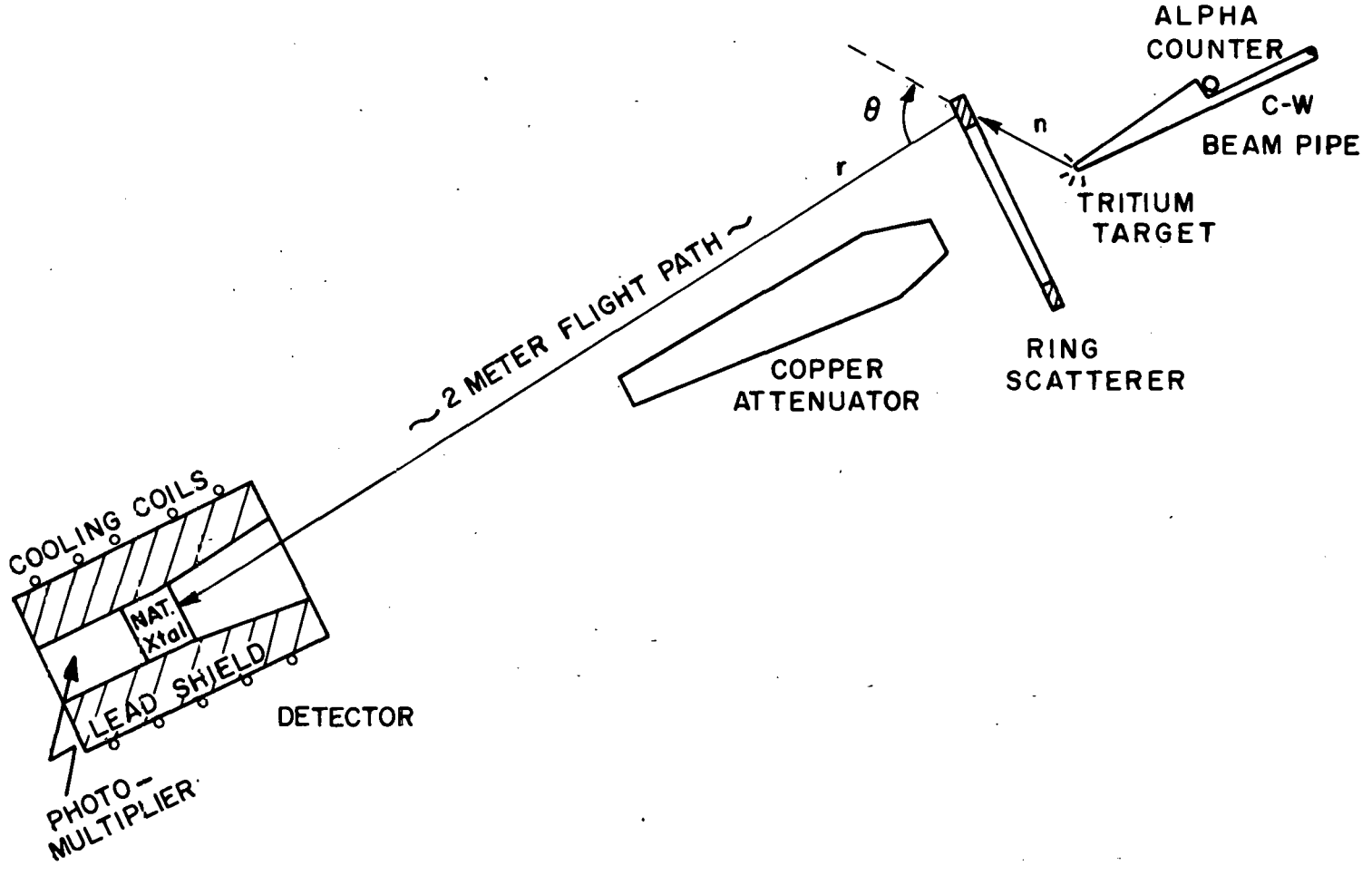

Fig. 1. Scattering geometry.

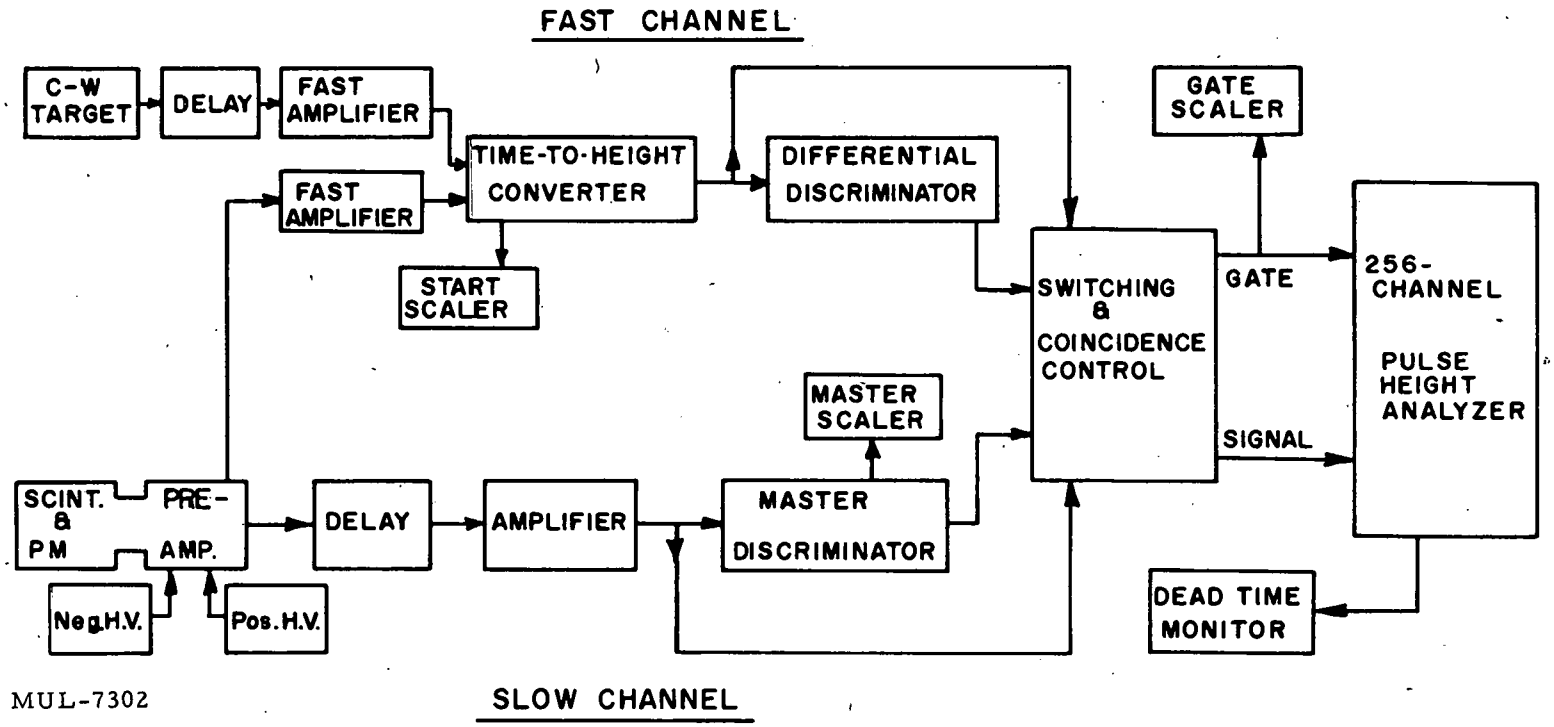

Fig. 2. Block diagram of detector electronics.

Negative voltage was applied across the first ten dynodes and positive voltage across the last four with the ground point at the tenth dynode.

The fast signal, after amplification by Hewlett-Packard wide-band amplifiers, entered a modified Los Alamos type[2] time-to-height converter as the "start" signal and triggered the discharge of a condenser. The zero-time Cockcroft-Walton target pulse was amplified and delayed and, upon entering the converter, served to stop the condenser discharge. This produced output pulses from the converter whose heights were proportional to the times of arrival of start pulses at the detector. By suitable use of the switching and coincidence control these output pulses could be analyzed and displayed on a 256-channel pulse-height analyzer. Such a "time spectrum" is shown in Fig. 3(A). As seen in the figure the difference between times of traversal of the approximately 2-meter flight path for the gamma rays and the elastically scattered 14-Mev neutrons was about 3.5×10^{-8} second. The converter output pulses could also be sent through a differential discriminator. When the output from the differential discriminator was used as a gate for the analyzer, the discriminator window could be visually set to bracket the gamma peak as shown in Fig. 3(B). This was the procedure used to select the gate pulses which allowed the analyzer to accept the slow signal just during that interval of time when gammas were being detected. To insure good time resolution the high voltages were adjusted so that the fast pulses produced by the 60-kev gammas from an Am^{241} source were saturated. Thus all pulses originating from gammas which deposited more than this energy in the scintillator should certainly be saturated. The leading edges of such signals which trigger the condenser discharge in the time-to-height converter, would have nearly identical rise times. A start signal discriminator at the input to the converter was set just below the Am^{241} peak to eliminate lower energy pulses with consequently longer rise times. During the selection of the timing gate the output of the differential discriminator was required to be in coincidence with the output of a master discriminator in the slow channel in order to reduce contributions from electronic noise. The master discriminator was set at the same level as the input discriminator of the multichannel analyzer.

In order to insure time coincidence between the differential discriminator gate pulses and the slow-channel signal pulse arriving at the

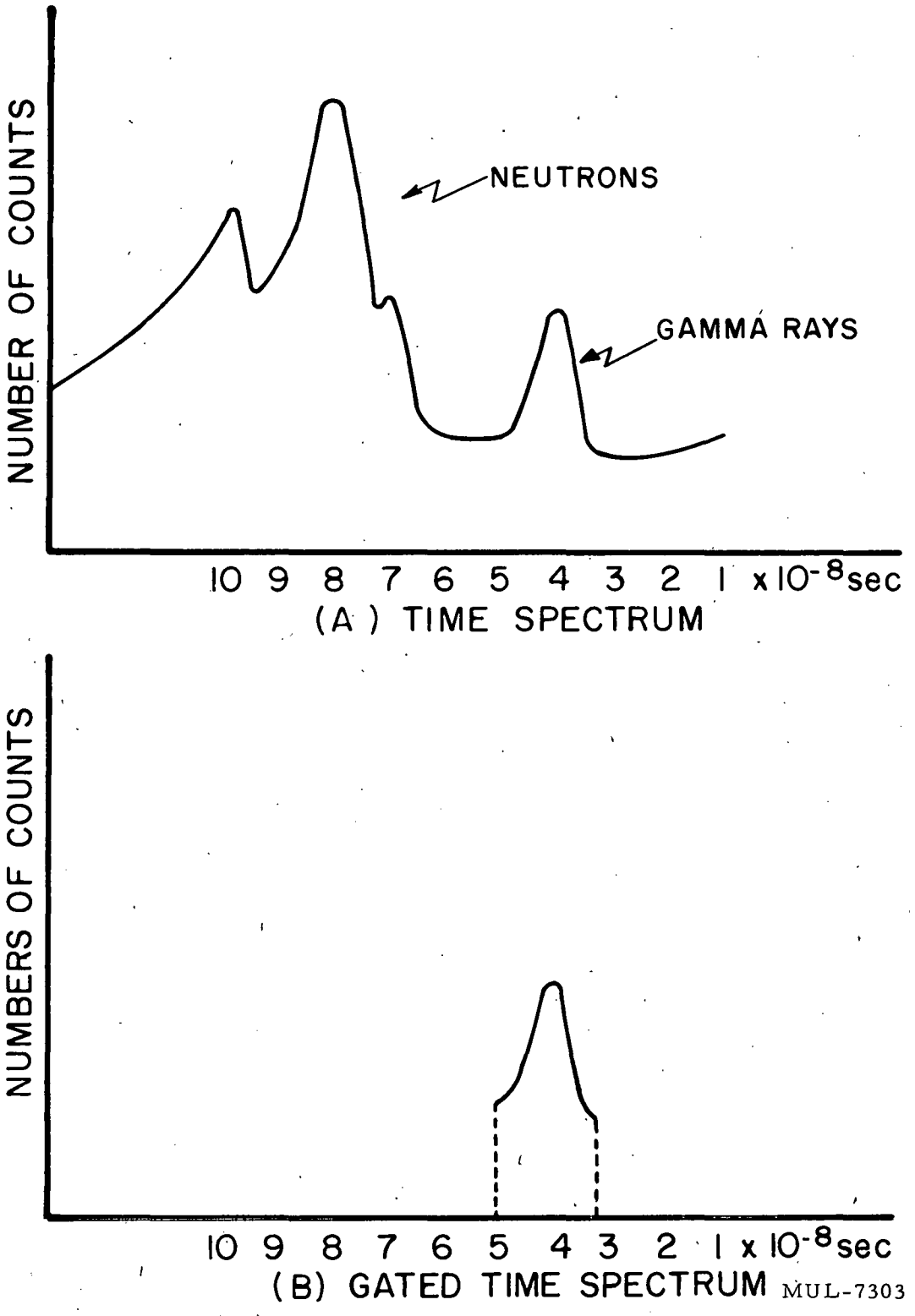

Fig. 3. Time and gated time spectra.

analyzer, delay was introduced in the slow channel until the 1-μsec signal pulse was well centered within the 2-μsec gate pulse. This provided enough overlap so that no signals were lost due to the small amount of jitter present.

Scalers at various points in the circuit enabled the counting of start, master, and gate pulses. The analyzer also had a scaler output indicating the dead time within the analyzer, and this, plus the information from the other scalers, was used to determine the total dead time of the detector-analyzer system. For an analysis and computation of this dead time see Appendix II.

PRELIMINARY AND AUXILIARY EXPERIMENTS

A number of preliminary and auxiliary experiments were performed which included the following:

1. Photopeak Efficiency - Measurements of the photopeak efficiency and the peak-to-total ratio as a function of energy for gamma-ray interactions in the shielded scintillator were made (see Appendix III). The precision of these measurements at the energy of the Be gamma ray was ± 4%.

2. Counting Rate - A thorough test of all electronic components to determine any possible change in gain of the system with varying counting rate was performed. No noticeable change in gain occurred for counting rates below 17 kc/sec. The counting rates actually used, however, were kept below this maximum by at least a factor of 4 so that the dead times in the time-to-height converter and the analyzer would be kept to reasonably low values.

3. Alpha Counter Calibration - If the D-T reaction is monitored by an alpha counter located at 90° with respect to the deuteron beam, the total neutron yield can be calculated from the number of observed alphas. It is very difficult, however, to calculate the neutron yield per 174°-alpha, since any errors in the input information to the calculations tend to become magnified at angles far from 90°. Therefore using a neutron detector as monitor, the number of alpha counts per neutron was measured for 90° and 174° assemblies separately. The ratio of these two numbers yields the 174° calibration constant in terms of the calculable 90° constant. Background in each counter (about 2% of the total counts), due mainly to the interaction of neutrons in the counter walls, was determined by introducing

a shutter in front of the entrance window. The ratio of the counts in the two counters was determined to within 1%. A complete description of this calibration procedure is described in UCRL-5619.[3]

4. Angular Distribution of Neutrons from the Target - An experimental measurement of the relative angular distribution of the neutrons from the target yielded the experimental points shown in Fig. 4. The theoretical curve is shown for comparison. Some of the features of the angular distribution may be understood as follows: (a) The observation that the anisotrophy is less pronounced than that of the theoretical curve is due partly to the fact that in the forward direction neutrons must penetrate the target backing (20 mils of tungsten). (b) The large dip near 90° is due to absorption of neutrons going edgewise through the target backing. (c) The rise observed at about 90° is due to the extra contribution of small-angle elastic scattering from the target disc.

5. Geometrical Effects - The possibility of target neutrons scattering from the Cu slug, and thus forming a secondary source of neutrons, was investigated. Although a difference of 1/2% between the number of neutrons received at a plastic scintillator located at various ring positions with the slug in and the number received with the slug out could have been detected, no effect was observed. Also, since it was inconvenient to remove the ring completely from its suspension in order to make background runs, it was moved to a position where it was essentially "out" both in time (signals would not arrive at the proper time to make a gate) and in space. In any event, the experimentally measured backgrounds with the ring in the out position and with the ring completely removed did not differ by more than 1/2%.

6. Crystal Activity - It was found that, if the neutron-induced activity in the NaI crystal (mainly from the 25-minute I^{128}) were allowed to build up for at least 25 minutes before taking data, the small number of counts which by chance occurred at the proper time to produce a gate was constant and could easily be subtracted with the rest of the background.

7. Energy Calibration - An energy calibration of the entire system was made using various radioactive sources with gamma rays of known energy. After such calibration the energies of unknown gamma rays could be determined with a precision of 1%.

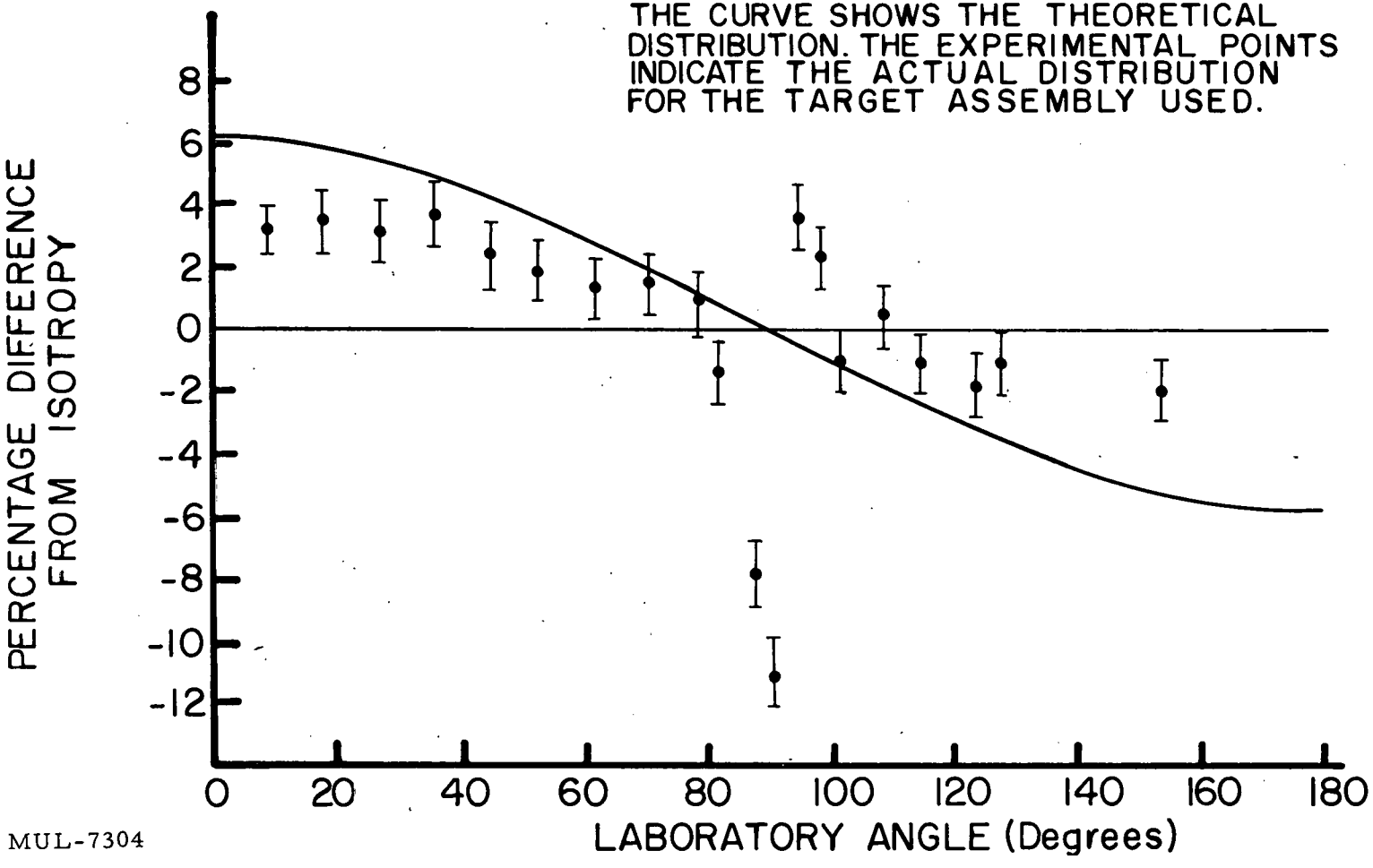

Fig. 4. Angular distribution of target neutrons.

PROCEDURE

Before every individual run all of the following routine checks were made: (a) The alpha spectrum was displayed on the multichannel analyzer; the gain was adjusted so that the alpha peak was located in a certain channel, and an integral discriminator was set on a "plateau" position. Observation of a similar spectrum after each run immediately showed any change in gain or discriminator setting. Any appreciable observed drift was cause for rejection of the run. (b) The gain of the entire detector-analyzer system was adjusted so that the photopeak of a Cs^{137} source occurred in a chosen channel of the analyzer. A check of the photopeak position immediately after a run showed whether any shift in gain had taken place. (The Cs^{137} source could be positioned in front of the counter, or removed, by remote control.) (c) The time spectrum was analyzed and the differential discriminator setting was examined for proper bracketing of the gamma peak.

The angular order of the runs was randomly staggered in order to expose any other possible change of conditions with time, since a monotonic change in angle coupled with a progressive change in some other parameter might result in a false asymmetry. Background runs were made every second angle run. Consistency of the background data gave an additional check on the stability of the entire system since the background was expected to remain constant with time.

After a run was completed the information in the analyzer was printed out on paper tape, and the readings on the clock and the various scalers were recorded. A picture of the spectrum displayed on the analyzer was taken with a Polaroid Land camera for quick reference before the final data were plotted.

TREATMENT OF THE DATA

Dead-time corrections (see Appendix III) were computed and applied to all raw data. The backgrounds were then subtracted and the corrected spectra were plotted. Base lines were then drawn under the peaks to separate each peak from the remainder of its spectrum. From drawing various reasonable base lines under the same peak it is estimated that a possible error of 7% could be introduced in the number of peak counts.

Monte Carlo calculations on an IBM 704 gave corrections for both multiple scattering of neutrons and self-absorption of gammas in the ring scatterer (see Appendix IV). The correction factors ranged from 1.25 at 30° to 1.15 at 150°. This variation with angle occurred because the energy of the incident neutrons was different at different angles and because the geometrical aspect which the ring presented to the neutron source changed with angle.

RESULTS

An example of the gamma-ray spectra produced by 14-Mev neutrons on beryllium is shown in Fig. 5. The simplicity of the spectrum may be understood from the following considerations: Of the energetically possible non-elastic neutron interactions, by far the major one is the (n,2n) process. (Ordinary inelastic scattering would leave Be^9 in a state unstable to neutron decay so that these events are just the prelude to (n,2n) processes.) Since the residual Be^8 is unstable to breakup into two alpha particles, for which no excited states have been observed, it is clear that this process yields no mechanism for the emission of gamma rays. The $Be^9(n,\alpha)$ reaction could conceivably leave He^6 in one of the excited states at 1.71 and 3.35 Mev but these too are unstable to particle decay. And finally, the Be(n, t) reaction could leave Li^7 in the well-known 0.477-Mev level which would subsequently emit a gamma ray of this energy. In fact, the gamma ray from this reaction is the only one observed. The part of the spectrum above, and a portion of the spectrum below, the 0.477-Mev line are due to gammas from the C-W target which were Compton-scattered in the Be ring. This background has no bearing on the cross sections reported in this paper because only the peak counts were used.

The differential cross section for the $Be^9(n, t')Li^{7*}$ reaction is displayed in Fig. 6. The horizontal wings on the points represent the angle subtended by the scatterer at the source; the vertical lines represent the uncertainty introduced by the measurement of the area under the 0.477-Mev gamma-ray peak.

Since the spin of the 0.477-Mev state in Li^7 is $J = 1/2$, the γ rays from this state must be isotropic, and the angular dependence observed

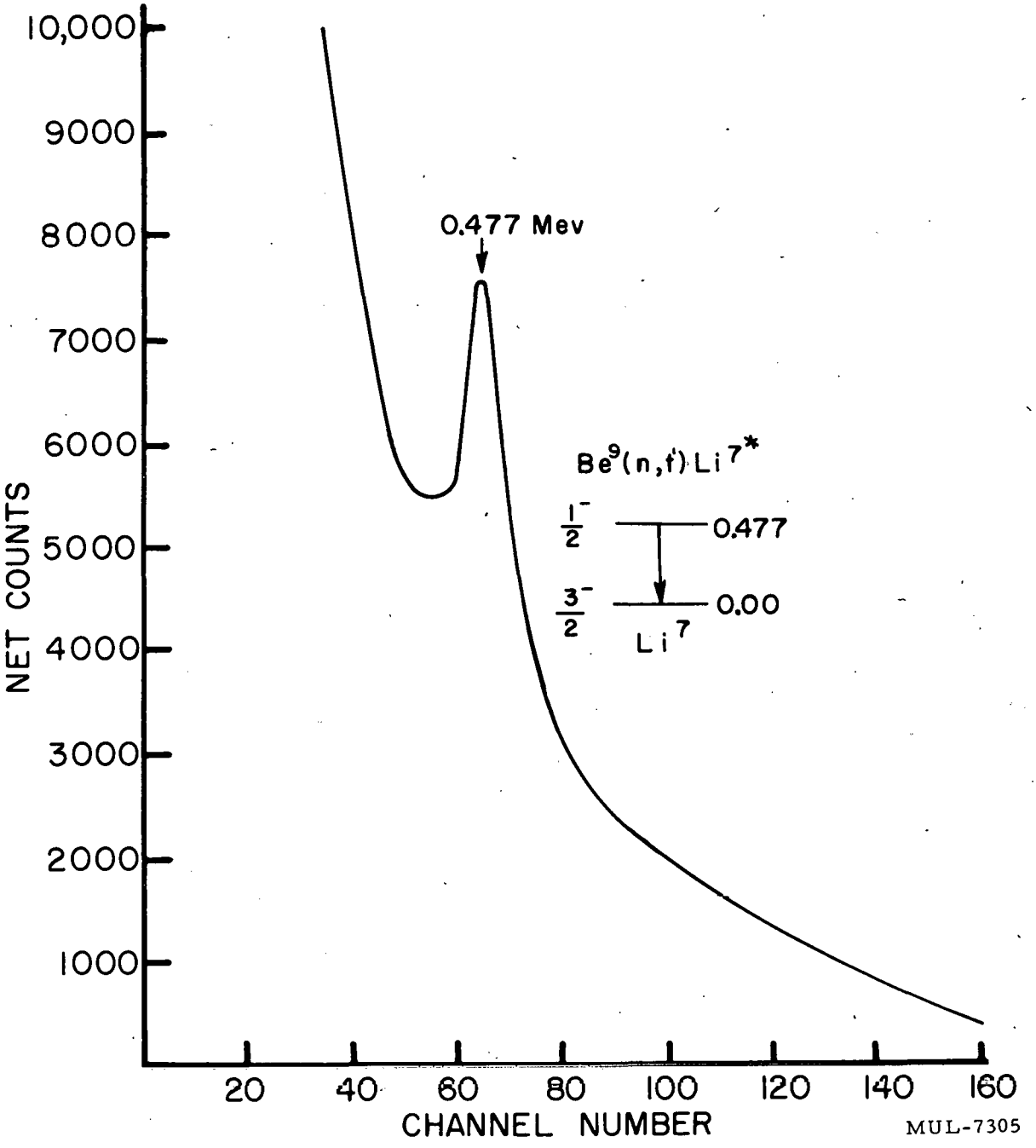

Fig. 5. Gamma-ray spectrum from beryllium.

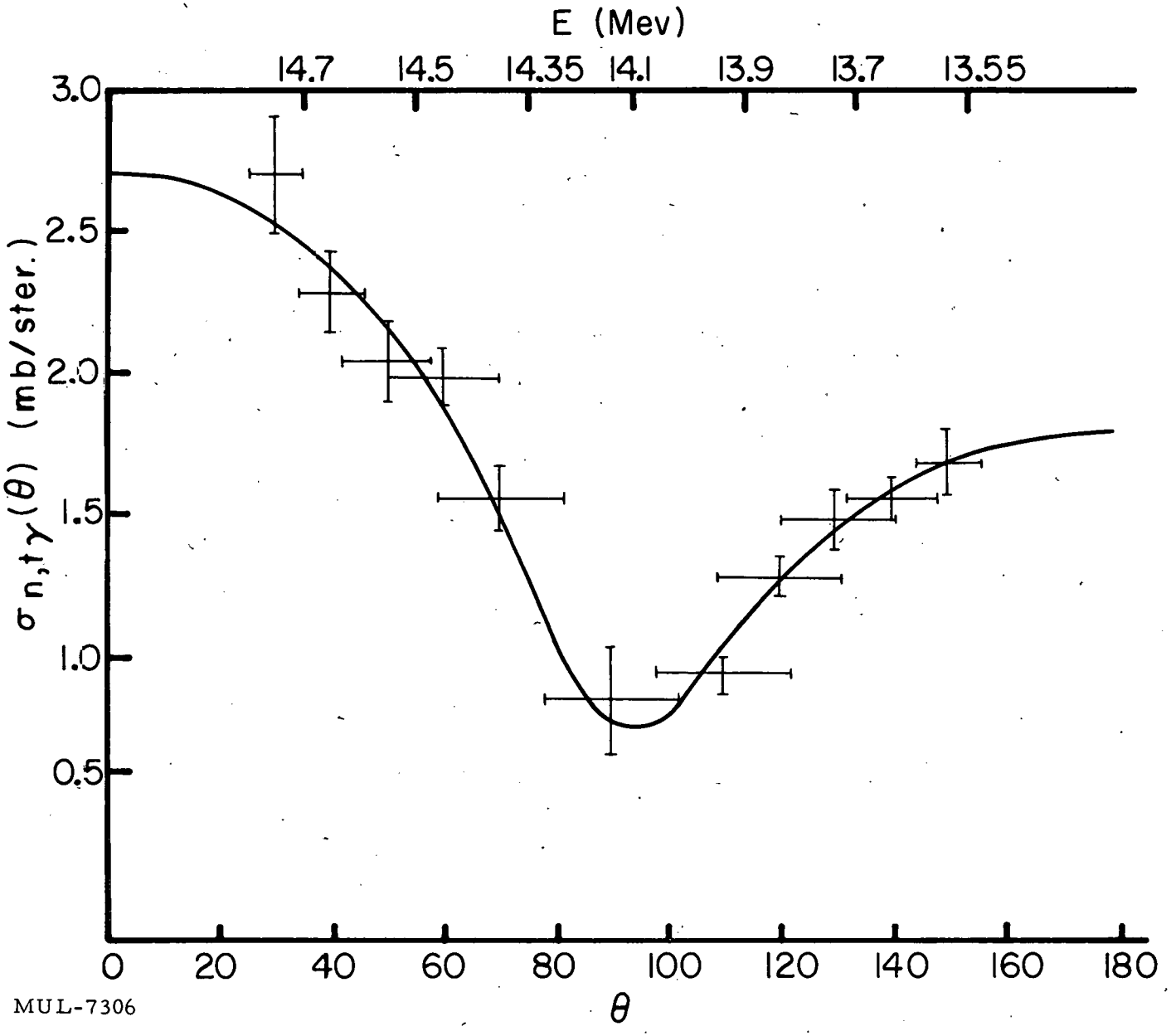

Fig. 6. Differential cross section for the $Be^{9}(n, t')Li^{7*}$ reaction.

should more properly be considered an energy dependence. Fig. 7 is obtained by multiplying each observed differential cross section by 4π and plotting the result versus incident neutron energy. The horizontal bars indicate the spread in incident neutron energy due to both the finite angle subtended by the scatterer at the source and the inherent energy spread[4] of neutrons emitted at any particular angle. The vertical lines represent the uncertainty introduced into each measurement as determined by the root-mean-square of the following individual sources of error:

1. Statistics contributed from 6 to 25% to the probable error.
2. The calibration of the neutron source and its angular dependence introduced about 2%.
3. The penetrability calculations used in the Monte Carlo determination of the contribution of secondary events introduced 3-5% error.
4. The determination of our detector efficiency for 0.477-Mev gamma rays introduced another 4%.

Other results pertinent to this investigation have recently been reported from LASL[5] and from Russia.[6] Although these two studies measured the total amount of tritium produced in the reaction (including transitions to the ground state as well as to the first excited state of Li^7), the data have been included in Fig. 7 for ease of comparison. The data indicates that the branching ratio

$$n + Be^9 \rightarrow \frac{t' + Li^{7*}\ (0.477)}{t + Li^7\ (\text{gnd.})} \approx 1.$$

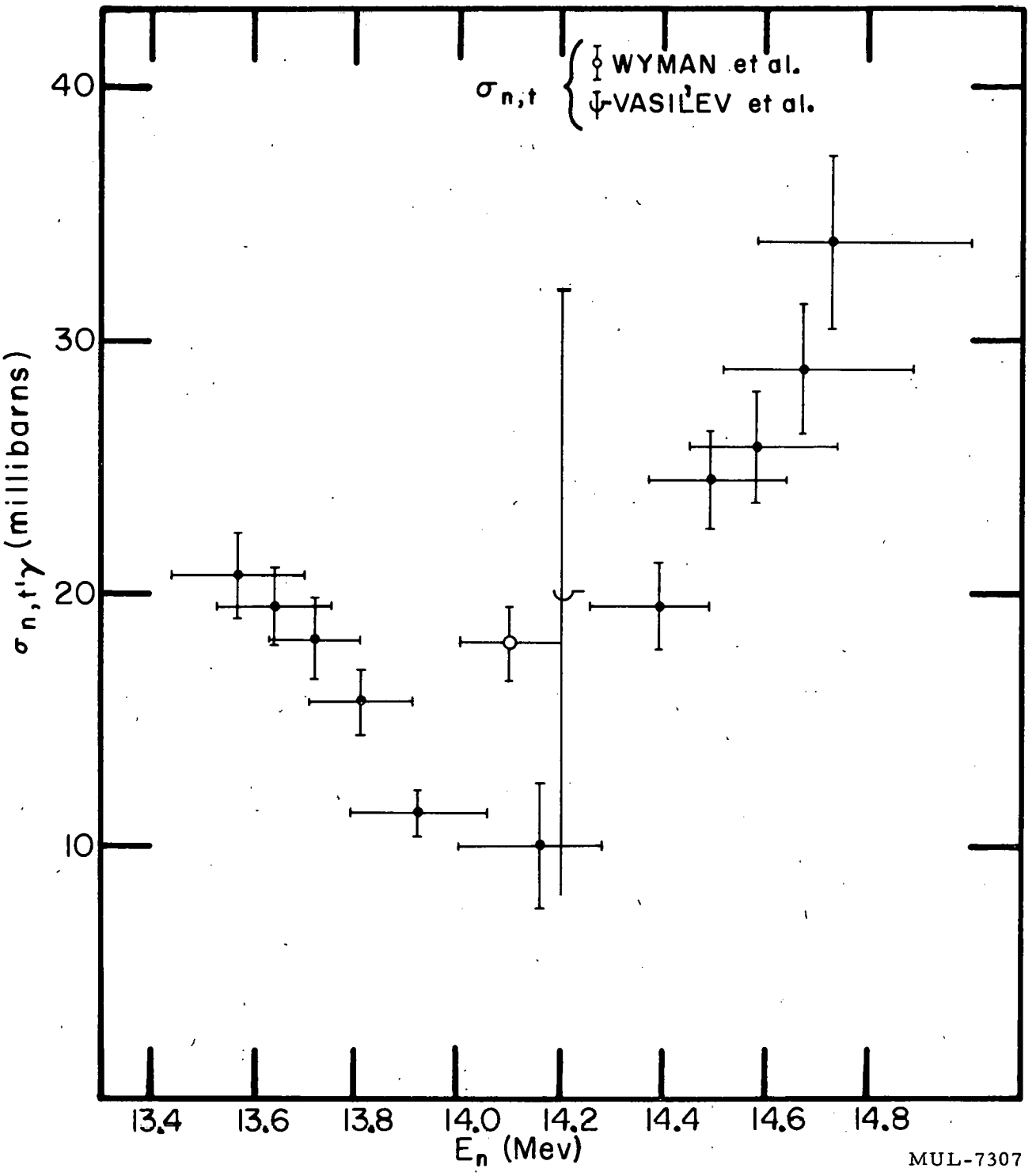

Fig. 7. Cross section for the $Be^9(n, t', \gamma)Li^{7*}$ reaction.

APPENDIX I

COCKCROFT-WALTON BUNCHE-SWEEPER SYSTEM

A schematic diagram of the system employed to produce short bursts of neutrons appears in Fig. 8. The beam from the Cockcroft-Walton accelerator passes through two sets of deflecting plates. A dc bias on one set of plates normally deflects the beam so that it cannot pass through a rather narrow slit in the beam pipe. When the phase between the voltages is adjusted so that the deuteron experiences an upward force at both sets of plates, as represented in Fig. 9, the beam is momentarily deflected into the slit. Thus bursts of deuterons, each about 2×10^{-8} second long, proceed toward the buncher at a 5 Mc/sec rate.

The buncher[8] is essentially a drift tube on which is impressed a 10 Mc/sec voltage which serves to modulate the velocity of the deuterons passing through. When the phase is properly adjusted the deuterons in the front portion of the burst are slowed down and those at the rear of the burst are speeded up, so that after a proper drift distance the deuterons are bunched to produce a burst about 3×10^{-9} sec long at the target.

APPENDIX II

DEAD TIME CONSIDERATIONS

In a detection system with dead time, the true counting rate is related to the observed counting rate through the relation

$$n_T = n_o + n_o n_T \tau, \tag{1}$$

where τ is the dead time. Our system has both a fast and slow channel. The dead-time analysis must consider the losses in each separately.

In the slow channel (see Fig. 10), the true counting rate at the analyzer input discriminator (also called trigger No. 1) is

$$n_{T,i} = \frac{n_{o,m}}{1 - n_{o,m} \tau_m}, \tag{2}$$

where the subscript m refers to the master discriminator. These counts are made up principally of neutrons and γ rays. Since there can be no selectivity, the fraction of γ rays which get through the input discriminator

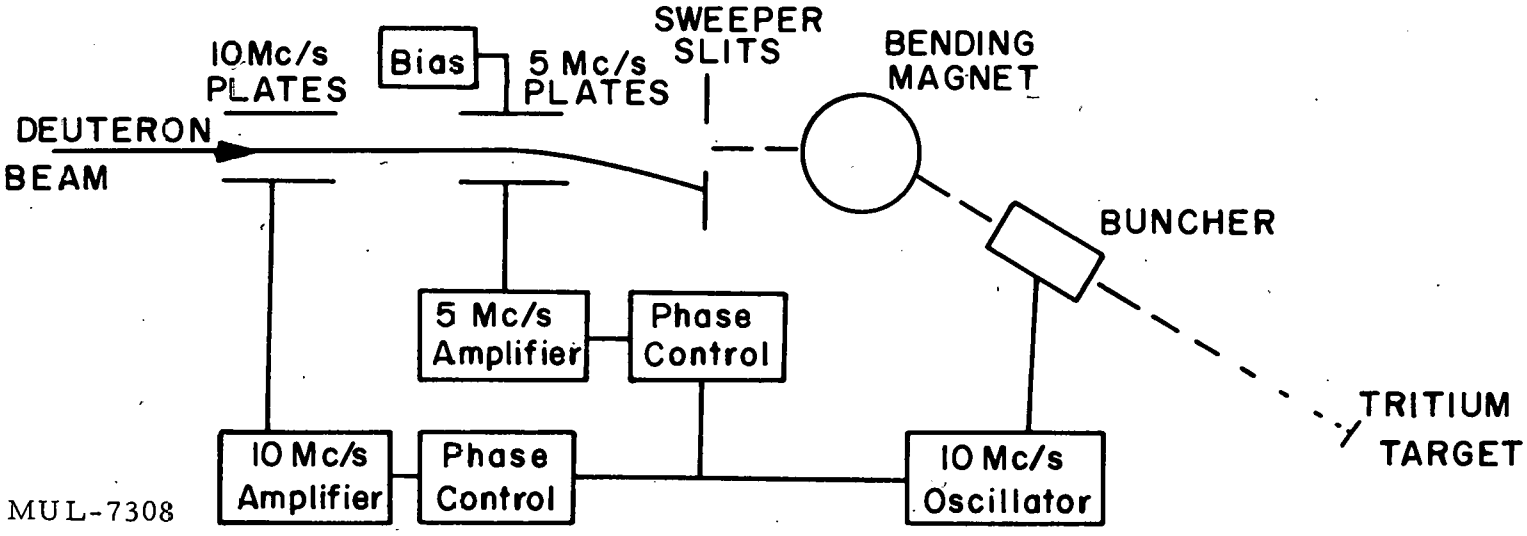

Fig. 8. Schematic of pulsing system.

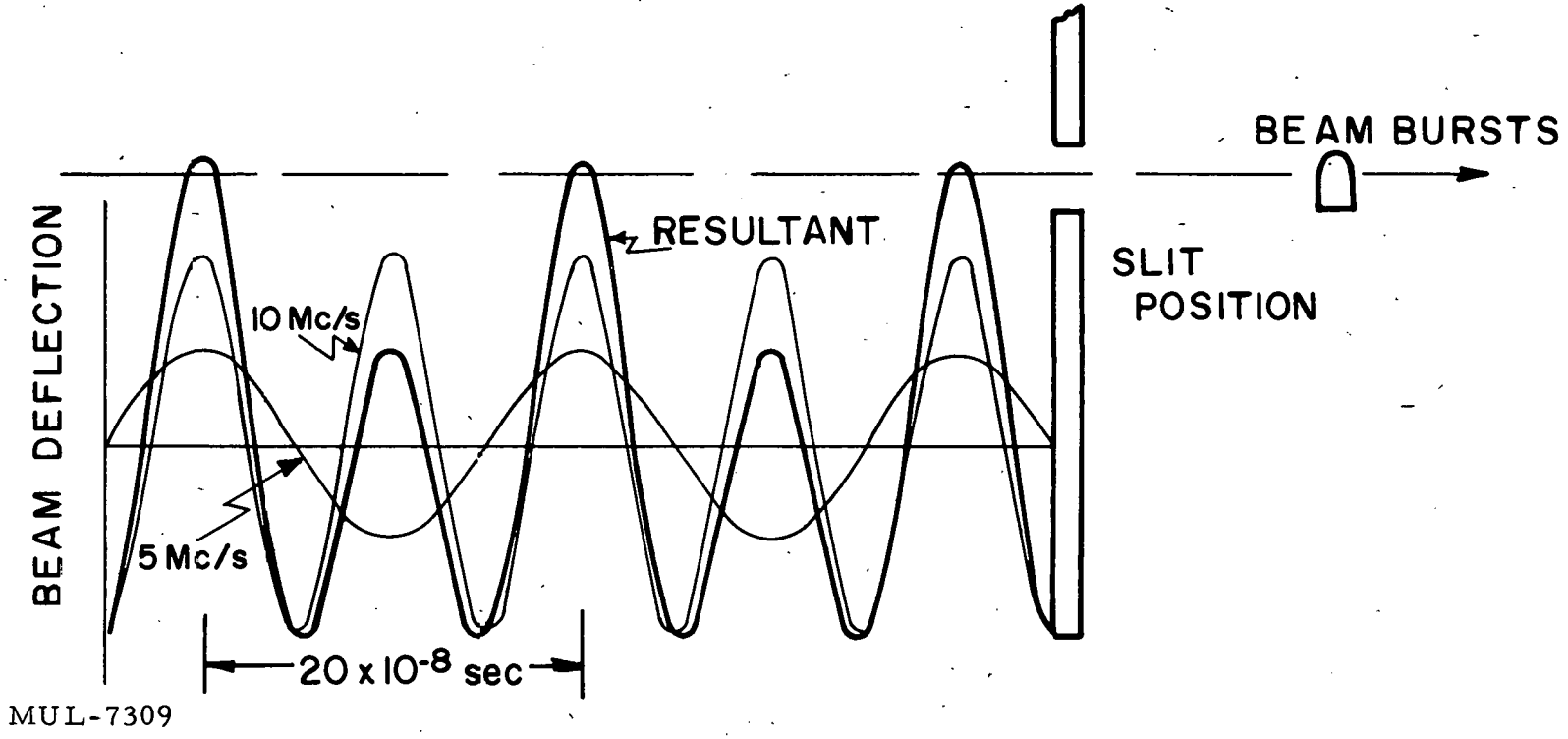

Fig. 9. Phasing of 5 and 10 Mc/sec sweeps.

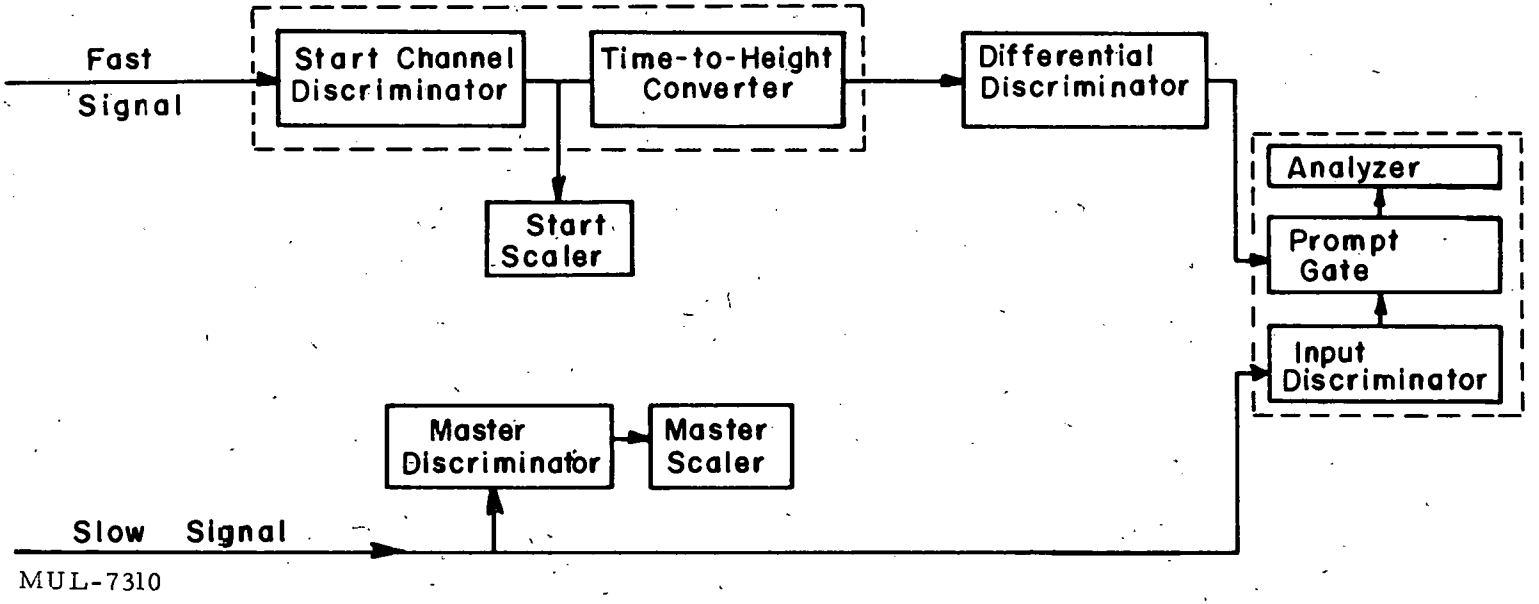

Fig. 10. Sources of dead time in fast and slow channels.

is the same as the fraction of total counts which get through:

$$f_i = \frac{n_{o,i}}{n_{T,i}} = \frac{1}{1 = n_{T,i}\tau_i} \quad . \tag{3}$$

This fraction enters the prompt gate.

In the fast channel the true input to the time-to-height converter is

$$n_{T,c} = \frac{n_{o,s}}{1-n_{o,s}\tau_s} \tag{4}$$

where the subscript s refers to the "start channel" discriminator. Again, both neutrons and γ rays contribute and the fraction of γ rays which get through the converter is

$$f_c = \frac{1}{1 + n_{T,c}\tau_c} \quad . \tag{5}$$

No further dead time is contributed by the differential discriminator unless the pulses occur within the proper time interval and they are separated by at least the dead time of the converter. This is because the dead time for pulses which do not get through the differential discriminator window is only the width of the input pulse. Since the number of pulses occurring within the proper time interval is about one-tenth the total, the extra dead time contributed by the differential discriminator is about 10% that of the time-to-height converter and so will be ignored.

The output from the differential discriminator proceeds to the prompt gate where a coincidence occurs with the slow-channel pulse. The probability that a pulse gets through the prompt gate is equal to the probability that it is not lost in either the slow channel or the fast channel, i.e., $f_c f_i$.

The gated pulses are then analyzed. Although the entering pulses are no longer quite random (i.e., no intervals of less than about 3 μsec, occur) the analyzer dead time (30 μsec plus 0.5 μsec/channel) is so much longer than this that they will be considered random and the fraction of the incoming pulses analyzed will be taken to be

$$f_a = \frac{1}{1 + n_{o,a}\bar{\tau}_a} \quad , \tag{6}$$

where $\bar{\tau}_a$ is the average dead time of the analyzer.

Thus the fraction of the γ counts not lost is

$$F = f_i f_c f_a \tag{7}$$

and the true counting rate is given by

$$n_T = \frac{n_o}{F}. \tag{8}$$

By neglecting all second-order terms and simplifying, the dead time factor becomes

$$\frac{1}{F} = 1 + n_{o,a}\bar{\tau}_a + n_{o,m}\tau_i + n_{o,s}\tau_c. \tag{9}$$

The quantity $n_{o,a}\bar{\tau}_a$ is obtained from the dead-time circuit (shown schematically in Fig. 11) associated with the analyzer. The dead-time

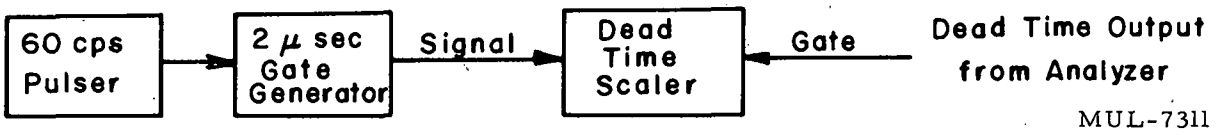

Fig. 11. Schematic of dead-time monitor.

scaler records 60-cycle pulses when it is gated on by pulses from the analyzer whose lengths are equal to the time the analyzer is dead. The coincidence rate of the 2-μsec 60-cycle pulses and the dead-time pulses at the dead-time scaler is given by

$$n_{o,d} = 60 n_{o,a}\left[\bar{\tau}_a + (2 \times 10^{-6})\right] \tag{10}$$

and thus

$$n_{o,a}\bar{\tau}_a = \frac{1}{60} n_{o,d} - (2 \times 10^{-6}) n_{o,a}. \tag{11}$$

If the total counts, N, recorded in time t (minutes), are used (e.g., $n_{o,d} = N_d/60t$ and $n_{o,a} = N_a/60t$), then the dead time correction factor becomes

$$\frac{1}{F} = 1 + \frac{1}{60t}\left[\frac{N_d}{60} - (2 \times 10^{-6})N_a + N_m\tau_i + N_s\tau_c\right]. \tag{12}$$

Dead times ranged from 3 to 5%. In a typical case, the separate contributions from the various sources amounted to 2.2% for the analyzer, 1.2% for the input discriminator, and 0.6% for the time-to-height converter.

APPENDIX III

CRYSTAL EFFICIENCY MEASUREMENTS

If the pulse-height spectrum is observed from a gamma-ray source of strength S, the total number of counts in the spectrum is

$$N_t = S\epsilon_t, \tag{13}$$

where ϵ_t is the total efficiency. The number of counts in the full-energy peak is

$$N_p = S\epsilon_p, \tag{14}$$

where ϵ_p is the so-called "photo peak efficiency."
Hence,

$$\epsilon_p = \frac{N_p}{N_t}\epsilon_t. \tag{15}$$

The total efficiency for a NaI crystal detector is calculable with a probable error of about 3% due to uncertainties in our knowledge of the gamma-ray absorption coefficients. Thus, photopeak efficiencies for monoenergetic gamma sources may be measured in terms of two observed numbers and an easily calculable efficiency.

For a source emitting two gamma rays in cascade, the above equations may be extended to

$$N_t = S(\epsilon_{t1} + \epsilon_{t2}) \tag{13a}$$

$$N_{p1} = S\epsilon_{p1} \qquad N_{p2} = S\epsilon_{p2} \tag{14a}$$

and

$$\epsilon_{p1} = \frac{N_{p1}}{N_t}(\epsilon_{t1} + \epsilon_{t2}) \qquad \epsilon_{p2} = \frac{N_{p2}}{N_t}(\epsilon_{t1} + \epsilon_{t2}), \tag{15a}$$

where the subscripts 1 and 2 distinguish the features of the two gamma rays. The case of Na^{22} may be treated in this way except for some minor complications. Here, we have positron emission followed by a γ ray of 1.28 Mev. However, two facts must be kept in mind: first, for each positron there is one 1.28-Mev γ ray, but two annihilation quanta, and second, 1.28-Mev gammas are emitted immediately after K-capture 10.5% of the time. Thus the above equations should be written:

$$N_t = S(0.90 \times 2)(\epsilon_{t1} + \epsilon_{t2})$$

$$N_{p1} = 1.8S\epsilon_{p1} \qquad N_{p2} = S\epsilon_{p2} \tag{14a'}$$

and

$$\epsilon_{p1} = \frac{N_{p1}}{N_t}(\epsilon_{t1} + 0.55\epsilon_{t2}) \qquad \epsilon_{p2} = \frac{N_{p2}}{N_t}(1.8\epsilon_{t1} + \epsilon_{t2}). \tag{15a'}$$

The spectrum of Fig. 12(A) was treated in this way. Figure 12(B) shows how it was possible to eliminate contributions from one of the γ rays with a coincidence circuit gating system.

If a shield is used to protect the crystal from stray radiation, the inscattering contribution made by the shield to the spectrum must also be considered. For example Eq. (14) would become

$$N'_p = S\epsilon'_p, \tag{16}$$

where the primes refer to numbers resulting from measurements made with the shield in place. Since the total efficiency for a shielded crystal cannot easily be calculated, Eq. (16) must be used in conjunction with Eq. (13), where N_t is found from measurements on an unshielded crystal, to give

$$\epsilon'_p = \frac{N'_p}{N_t}\epsilon_t \tag{17}$$

for the photopeak efficiency of the shielded detector.

The actual number of counts observed depends, of course, on the source-to-crystal distance and the geometrical orientation of the crystal with respect to the source. In the neutron-Be experiment, the gamma-rays were produced in a scattering ring which was used at distances between 75 in. and 95 in. from the face of the crystal along a line that was an extension of the crystal axis. The segments of the ring were about 4° off this axis. Thus, a preliminary experiment was performed to find the variation of crystal efficiency over the ranges of our geometrical setup. Since the distance variation amounted to less than 1/2% and since the off-axis efficiency differed from the on-axis efficiency by only 1/4%, the total efficiency calculations were coded for an on-axis source at the average distance, and the experimental measurements were made under similarly simplified conditions.

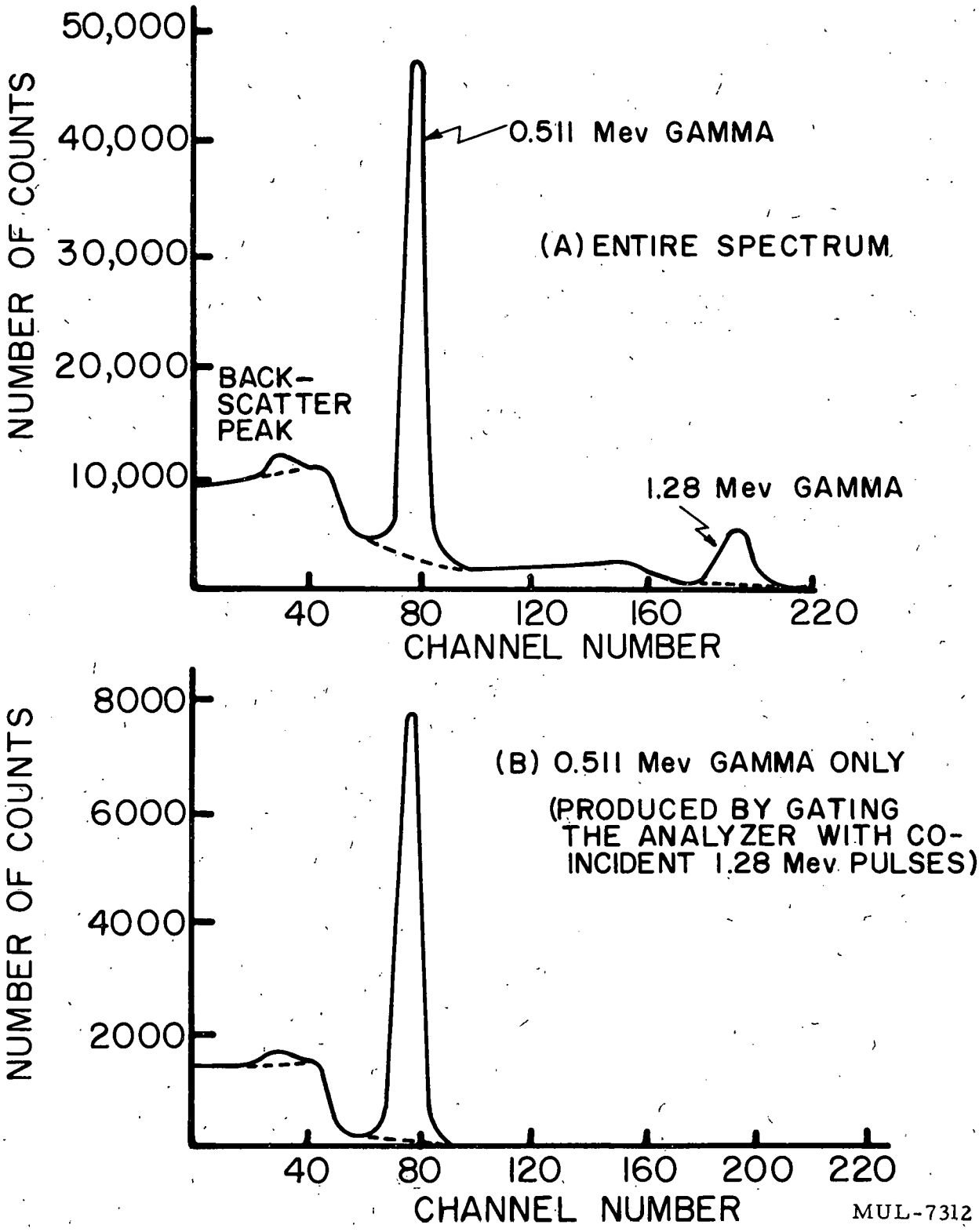

Fig. 12. Gamma spectra from Na^{22}.

A list of the sources used and their gamma-ray energies is given in Table I. The sources were thin in order to reduce self-scattering. Both the source and the detector were suspended 5 ft above the thin aluminum floor far from the ceiling and walls. Background counts were taken by introducing an 18-in.- long copper slug between the source and the detector. Since it was found necessary to shield the crystal with lead during the neutron runs, the efficiency measurements were made both with and without the shield.

Table I. Gamma-ray sources used in efficiency measurements.

Source	E (Mev)
Hg^{203}	0.280
Na^{22}	0.511 and 1.28
Cs^{137}	0.663
Na^{24}	1.37 and 2.75

In order to compare properly the experimental unshielded crystal efficiency with the theoretical efficiency, corrections had to be made in the treatment of the data to eliminate the effect of gamma-ray interactions in the photomultiplier tube and its base. This appeared as a back-scattering peak (about 2% of the total spectrum) which was subtracted to give a smooth residual curve.

An independent determination of source strength compared with a source strength calculation based on Eq. (1) yields a check on the precision of the method. Our own calculations of the strength of a Cs^{137} source gave a value which differed by less than 1% from that obtained with an ionization chamber[9] which had previously been calibrated with a National Bureau of Standards source. The agreement is well within the precision of both measurements.

In measuring ϵ_p the major contribution to the experimental error (about 1.5% at 0.3 Mev and 6% at 2.75 Mev) was due to the uncertainty in isolating the peak counts from the remainder of the spectrum. This isolation (see Fig. 12) was done in the same manner that was to be used in separating the peaks from the continuum in the neutron-produced γ-ray spectra so that all the work reported here is internally consistent. It should be noted that, before comparison of photopeak efficiencies reported

by different authors can be made. It is necessary to know the method used to distinguish the peak counts.

The final curves of peak efficiency as a function of energy are shown in Fig. 13 where the vertical bars on the points represent the total estimated probable error due to both experimental and theoretical uncertainties.

APPENDIX IV

MULTIPLE SCATTERING CORRECTIONS TO CROSS-SECTION CALCULATION

Because the scattering-ring cross section has dimensions of about one-half mean-free-path for 14-Mev neutrons, the correction for events caused by secondary processes is important. The gamma-ray-producing event is the

$$Be(n, t')Li^{7*} \rightarrow Li^{7} + \gamma\ (0.477)$$

reaction with threshold at 12.1 Mev. Since the (n, 2n) process invariably leaves residual neutrons with less than this energy, this process cannot make subsequent contributions to the reaction in question. However, elastically scattered neutrons will, in general, be capable of contributing to the $Be(n, t')Li^{7*}$ events, although, because of the small mass of the Be nucleus, the elastically scattered neutrons will have a somewhat lower energy than that of the neutron originating at the source.

Because only elastic scattering can contribute to the secondary events and the threshold for the reaction is high, the correction calculations are relatively simple.

Assuming a point source of neutrons, isotropic over the solid angle subtended by the scattering ring, a Monte Carlo calculation was performed to determine the following neutron collision probabilities:

P_n - the probability that a neutron which enters the ring makes a non-elastic collision

E_{2n} - the expected number of non-elastic collisions per entering neutron which are made by neutrons already having made at least one elastic collision

$p_{1n}(\rho, z)$ - the probability that a neutron making its first non-elastic collision in the ring will make that collision in the space interval $\rho, \rho + \Delta\rho$; $Z, Z + \Delta Z$. (see Fig. 14)

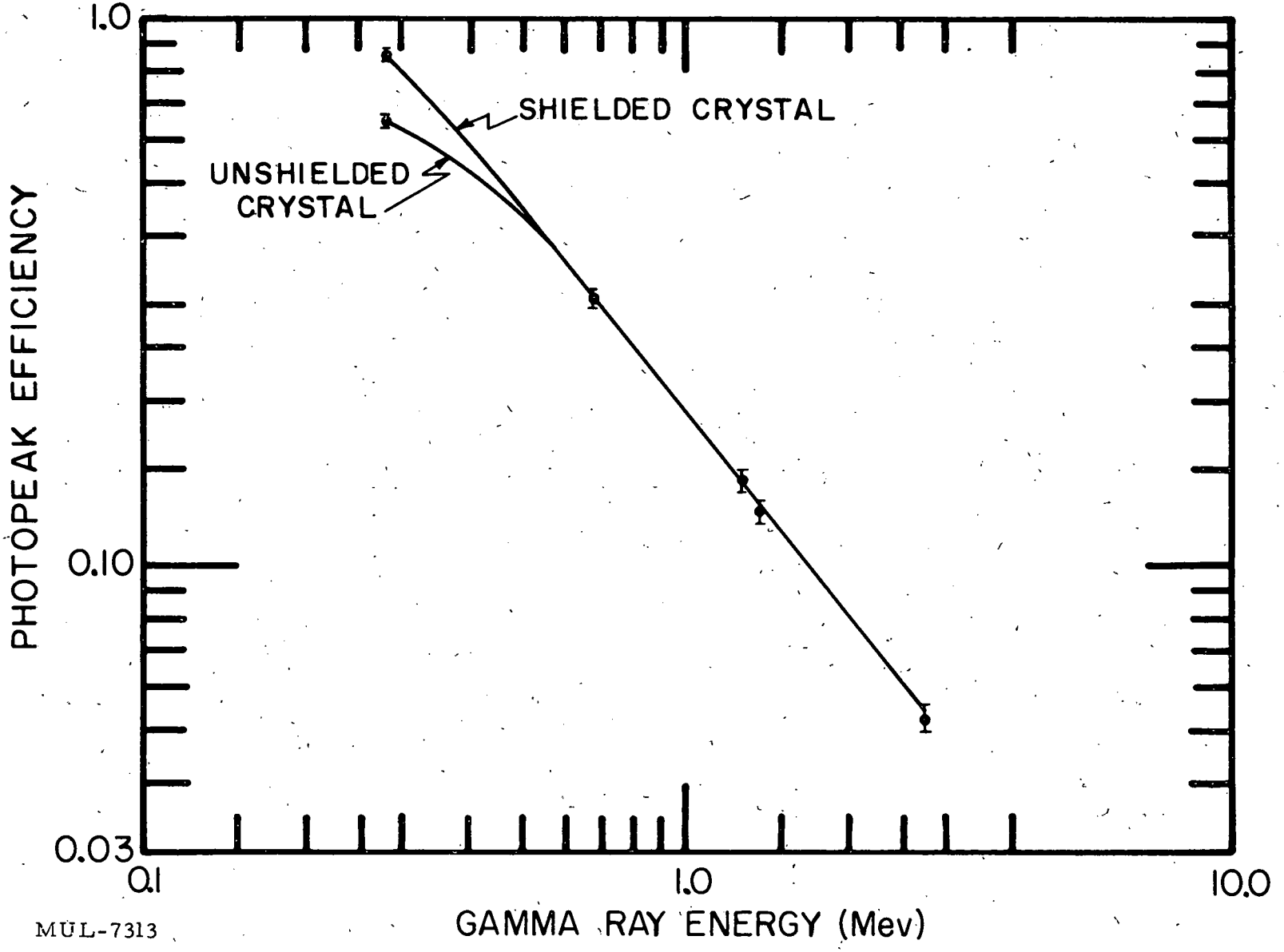

Fig. 13. Peak efficiency of NaI crystal.

$p_{2n}(\rho, Z, \epsilon)$ - the probability that a neutron with energy in the interval $\epsilon, \epsilon + \Delta\epsilon$ making a non-elastic collision in the ring other the first, will make that collision in the interval $\rho, \rho + \Delta\rho$; $Z, Z + \Delta Z$.

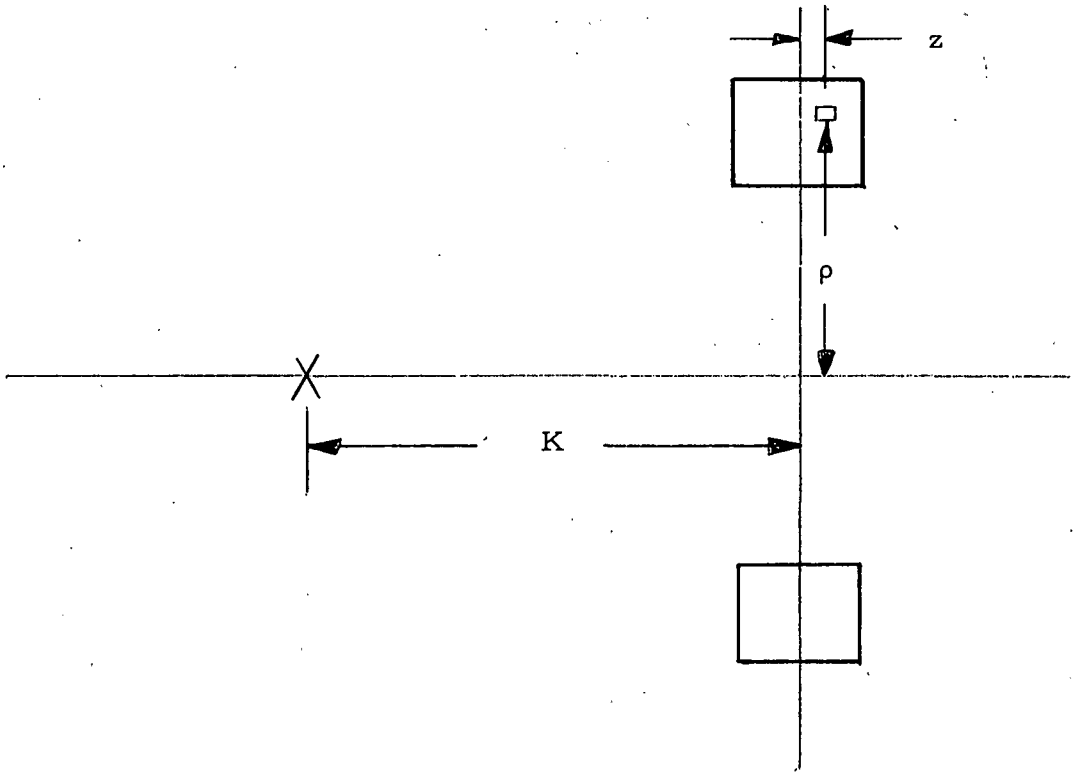

Fig. 14

The method of calculation involves a generation of chains of neutron collisions. From the collision chains estimates of the expected values of certain random variables are made. These expected values are equal to P_n, E_{2n}, p_{1n}, and p_{2n}.

In a typical run on the IBM 704 computer, case histories of 10^4 neutrons are collected in less than 10 minutes. The data obtained for a ring position corresponding to a scattering angle of 70° are pictorially represented in Fig. 15.

0.0561 ±0.0020	0.0309 ±0.0020	0.0265 ±0.0018	0.0243 ±0.0018
0.0653 ±0.0024	0.0456 ±0.0024	0.0427 ±0.0023	0.0335 ±0.0020
0.0857 ±0.0030	0.0680 ±0.0029	0.0626 ±0.0028	0.0586 ±0.0023
0.1125 ±0.0036	0.1045 ±0.0036	0.0977 ±0.0032	0.0855 ±0.0021

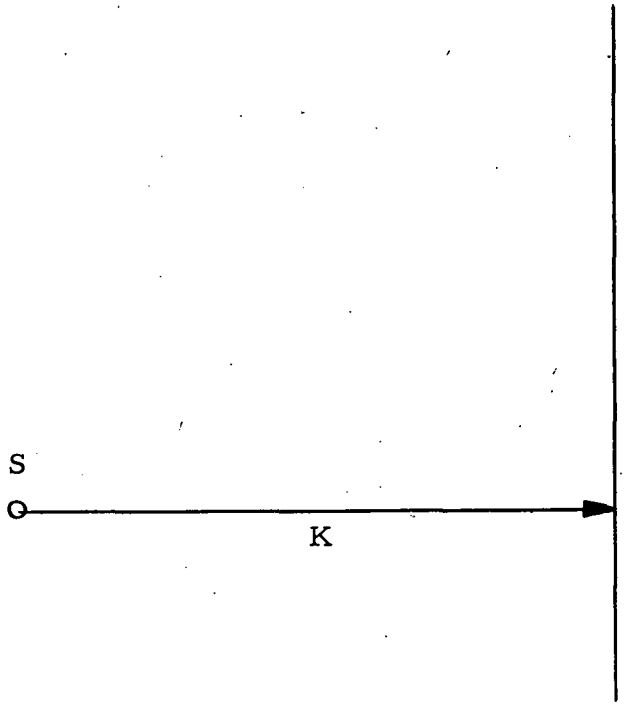

K = axial distance from neutron source to center of scattering ring = 6.18cm

$\theta = 70°$

ϵ_o = incident neutron energy = 14.4 Mev

$P_n = 0.1585 \pm 0.0006$

Fig. 15. Cross section of Be Ring, showing p_{1n} values.

The Figure represents a cross section of the Be scattering-ring which has been subdivided into 16 equal-volume elements (the sub-areas shown are not necessarily equal). The numbers in each square indicate the probability and its uncertainty for a first non-elastic collision in the region defined by the square. In our convention $\sum_i p_{1n}(i) = 1$ (where i identifies the volume element) so this sum must eventually be normalized to P_n.

In calculating the p_{2n} distribution the scattering-ring cross section was divided into four equal volume parts. This allowed us to maintain reasonably good statistics for the numbers in the p_{2n} table with 10^4 incident neutrons (see Fig. 16). Also it was established that the error introduced in the cross-section measurement by neglecting the effect of the coarse-grain calculation on the correction term was inconsequential. In our convention $\sum_{i,\epsilon} p_{2n}(i, \epsilon) = 1$ so this sum must be normalized to E_{2n}.

It must be kept in mind that after at least one elastic scatter the neutron has less than its original energy and since at threshold the cross section for the interesting event must be zero, it is clear that the cross section for producing a gamma ray in a secondary process may be quite different than that for a primary process. In order that only one unknown cross section appear in the expression describing the gamma-ray production we introduce the term

$$r(\epsilon) = \frac{\sigma_{nt'}(E)}{\sigma_{nt'}(E_o)} \tag{18}$$

Once $r(\epsilon)$ has been determined, each number in the p_{2n} table is multiplied by the appropriate $r(\epsilon)$ to determine the true contribution of the secondary process to the interesting events.

$$E_{2n} = 0.0448 \pm 0.0007$$

ϵ_n	p_{2n} Table	
14.2 - 14.4	0.1097 ±0.0056	0.1083 ±0.0058
	0.0812 ±0.0050	0.0848 ±0.0048
14.0 - 14.2	0.0529 ±0.0038	0.0588 ±0.0041
	0.0449 ±0.0037	0.0411 ±0.0033
. . .	. . .	. . .
12.55 - 12.76	0.0075 ±0.0013	0.0048 ±0.0011
	0.0058 ±0.0013	0.0076 ±0.0014
12.35 - 12.55	0.0048 ±0.0010	0.0050 ±0.0011
	0.0028 ±0.0008	0.0050 ±0.0010

Fig. 16. The distribution of secondary non-elastic collisions at energies other than the incident energy.

$r(\epsilon)$ was calculated on the assumption that the behavior of the cross section for a few Mev above threshold was adequately described by the penetrability of the reaction products, t' and Li^{7*}, through the Coulomb barrier.

The transmission coefficient for a particle of orbital angular momentum is given by [10]

$$T_\ell = \frac{4S_\ell KR}{\Delta_\ell^2 + (S_\ell + KR)^2}, \tag{19}$$

where

$$\Delta_\ell = R\left[\frac{G_\ell\left(\frac{dG_\ell}{dr}\right) + F_\ell\left(\frac{dF_\ell}{dr}\right)}{G_\ell^2 + F_\ell^2}\right] r = R$$

$$S_\ell = R\left[\frac{G_\ell\left(\frac{dF_\ell}{dr}\right) - F_\ell\left(\frac{dG_\ell}{dr}\right)}{G_\ell^2 + F_\ell^2}\right] r = R$$

$$= kRv_\ell,$$

since $$G_\ell\left(\frac{dF_\ell}{dr}\right) - F_\ell\left(\frac{dG_\ell}{dr}\right) = k$$

and $$\frac{1}{G_\ell^2 + F_\ell^2} \equiv v_\ell.$$

The functions F_ℓ and G_ℓ have been evaluated and tabulated by Bloch, et al.[11]

For low energies ($k \ll K$, S_ℓ and $\Delta_\ell \ll KR$),

$$T_\ell \rightarrow \frac{4S_\ell}{KR} = \frac{4k}{K} v_\ell. \tag{20}$$

The transmission coefficient depends sensitively on the value selected for the nuclear radius. There is evidence[10] which suggests that radii of light nuclei may be expressed as

$$R = 1.45\, A^{1/3} \times 10^{-13} \text{ cm.}$$

This yields for the radius of the Li^7 nucleus

$$R = 2.7 \times 10^{-13} \text{ cm.}$$

We adopt this value for the lithium nucleus in its first excited state also.

Calculations made for both $\ell = 0$ and $\ell = 1$ particles showed (on Fig. 17) that the penetrability of the latter was less than one-third that of the former, and that the energy dependence was not much different in the significant region. Because it was considered unnecessary to refine the correction calculation further, only the $\ell = 0$ results were used. In addition T_o was calculated assuming $R = 3.0 \times 10^{-13}$ cm. However, the energy dependence turned out to be so severe that we would certainly have observed it experimentally, had it existed. Thus we have used our calculated penetrabilities and the observed asymmetry of our angular distribution in a self-consistent way to establish confidence in our estimate of the nuclear radius. It is estimated that the uncertainty in the calculated energy dependence of the transmission coefficient could introduce an error of perhaps 20% in the correction for secondary events. This could contribute an error of as much as 5% in the differential cross section.

To calculate the self-absorption of gamma rays in the Be scattering-ring we assume that the gamma-source density is uniform within each subsection. Since the physical arrangement of our scattering system is such that the gammas never make an angle greater than 4° with the normal to the front crystal face, it is further assumed that the gamma rays proceed through the material along the normal to the front face of the scattering-ring.

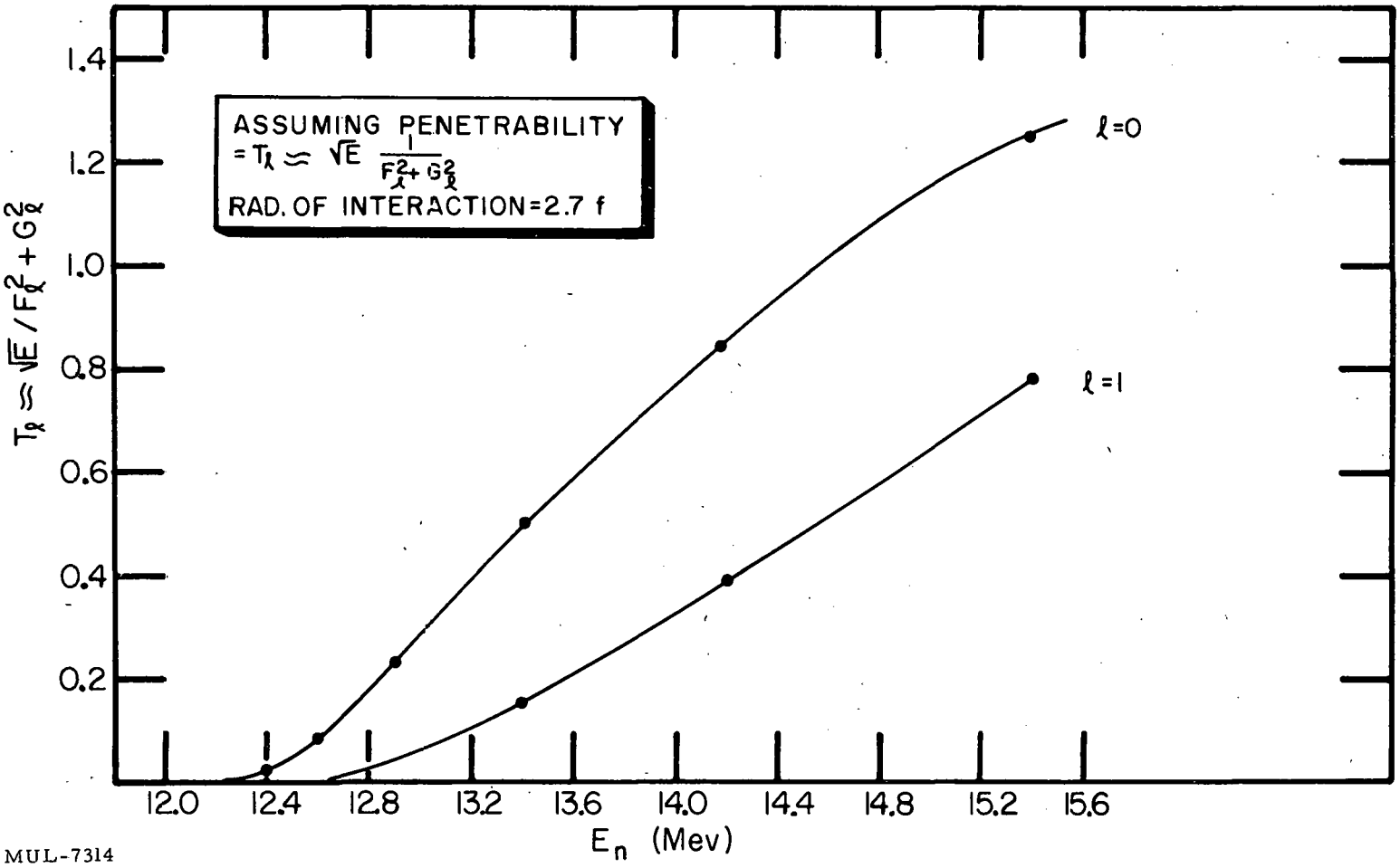

Fig. 17. Calculated shape of $\sigma n, t'$ for $Be^9(n, t')Li^{7*}$.

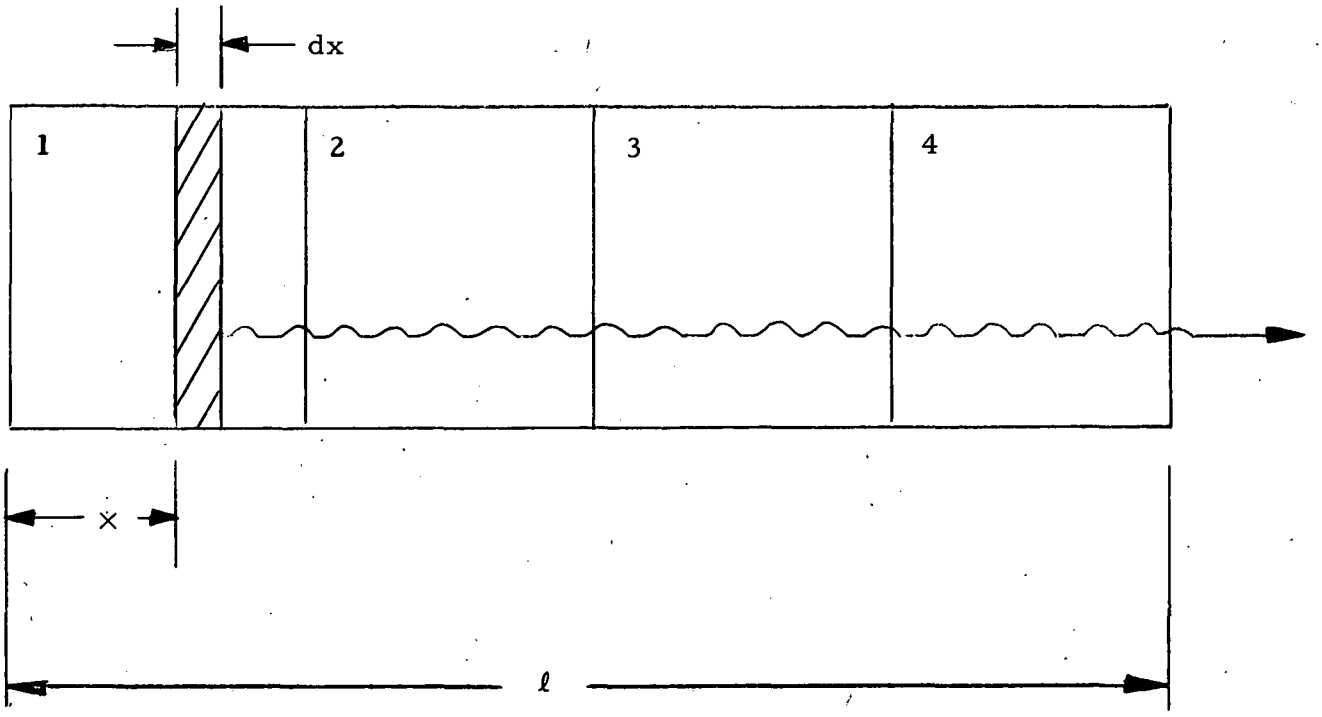

Let η_1 be the number of gamma rays (which proceed in the proper direction) originating per unit length so that $\eta_1 \frac{\ell}{4} = N_1$ (the total number produced in section 1). Of those originating in dx, the number emerging without having suffered an interaction is

$$dn_1 = \eta_1 \, dx \, e^{-\mu(\ell - x)} = \frac{N_1}{\ell/4} e^{-\mu(\ell - x)} \, dx, \tag{21}$$

so that of those originating in the entire section 1, the number emerging without having suffered an interaction is

$$n_1 = \int_0^{\ell/4} \frac{N_1}{\ell/4} e^{-\mu(\ell - x)} dx = \frac{N_1}{\mu\ell/4} e^{-\mu\ell} (e^{\mu\ell/4} - 1), \tag{22}$$

where μ is the total absorption coefficient. For 0.477-Mev gamma rays in Be, $\mu = 0.219 \text{ cm}^{-1}$.

Similarly for the other sections:

$$n_2 = \frac{N_2}{\mu\ell/4} e^{-3/4\mu\ell} \left(e^{\mu\ell/4} - 1 \right)$$

$$n_3 = \frac{N_3}{\mu\ell/4} e^{-\mu\ell/2} \left(e^{\mu\ell/4} - 1 \right)$$

$$n_4 = \frac{N_4}{\mu\ell/4} e^{-\mu\ell/4} \left(e^{\mu\ell/4} - 1 \right)$$

For each section, we define the absorption factor for the gamma rays as

$$\Gamma_1 = \frac{n_1}{N_1} = \frac{e^{-\mu\ell}}{\mu\ell/4} \left(e^{\mu\ell/4} - 1 \right) , \tag{23}$$

etc.

To write an expression for the number of gamma rays observed from the Be (n, t') reaction we introduce the following terms:

$N(\theta)$ is the number of neutrons incident on the Be scattering-ring. Although we have assumed that the neutron source is isotropic over the solid angle subtended by the scatterer, the fact that the source is not isotropic and that the source strength will vary for different positions of the scattering-ring was taken into account.

a is the area of the crystal detector and m the distance from the scattering-ring to the detector, so that a/m^2 is the solid angle subtended by the detector at the source of gamma rays.

ϵ'_p is the peak efficiency of the detector for the gamma rays in question. The prime indicates that the "shield effect" has been taken into account.

Then the number of gamma rays observed by the detector is

$$\mathcal{N}_{n,t',\gamma}(\theta) = \left[\sum_i N(\theta)\, p_{1n}(i) \frac{\sigma_{nt'}(\theta)}{\sigma_{nX}} \Gamma_i + \sum_{j,\epsilon} N(\theta)\, p_{2n}(j,\epsilon)\, r(\epsilon) \frac{\sigma_{nt'}(\theta)}{\sigma_{nX}} \Gamma_j \right] \frac{a}{m^2} \epsilon'_p , \tag{24}$$

where the first term expresses contributions from primary interactions and the second term, from secondary and higher order interactions. The sum is made over the various subsections of the scattering-ring.

$$\mathcal{N}_{n,t',\gamma}(\theta) = N(\theta)\frac{\sigma_{nt'}(\theta)}{\sigma_{nX}}\left[\sum_i p_{1n}(i)\Gamma_i + \sum_{j,\epsilon} p_{2n}(j,\epsilon)\Gamma_j\right]\frac{a}{m^2}\epsilon'_p$$

$$= N(\theta)\frac{\sigma_{nt'}(\theta)}{\sigma_{nX}} P_1\left(1+\frac{P_2}{P_1}\right)\frac{a}{m^2}\epsilon'_p, \qquad (25)$$

where $P_1 = \sum_i p_{1n}(i)\Gamma_i$

$$P_2 = \sum_{j,\epsilon} p_{2n}(j,\epsilon)\, r\,(\epsilon)\Gamma_j .$$

The desired cross section may be expressed

$$\sigma_{nt'}(\theta) = \sigma_{nX}\frac{\mathcal{N}_{nt'\gamma}(\theta)}{N(\theta)\, P_1\left(1+\frac{P_2}{P_1}\right)\frac{a}{m^2}\epsilon'_p}. \qquad (26)$$

The non-elastic cross section appears prominently in this development and it might seem that the cross section for the reaction in question may depend on the precision with which the non-elastic cross section is known. In fact, however, P_1 is proportional to σ_{nX}, and since the number of gamma rays produced is proportional to the product of P_1 and $\sigma_{nt'}/\sigma_{nX}$, the number used for the non-elastic cross section essentially cancels. This does not mean that an arbitrary number may be used in its place since the distribution computed will depend on the number used for the ratio of elastic to non-elastic cross sections. At any rate, the effect of any uncertainties in σ_{nX} on the final $\sigma_{nt'}$ will be very weak.

ACKNOWLEDGMENTS

It is a pleasure to acknowledge the invaluable contributions of Dr. Donald H. Davis to the analysis of the multiple scattering phenomenon. We would also like to express our gratitude to A.B. Williams who helped with much of the data analysis, to Vernon Ehlers who helped in the early phases of the work, and to the operating crew of the Cockcroft-Walton Accelerator under the capable guidance of Roy V. Cederlund. Finally, we express our appreciation for mechanical engineering support fron H.E. Brooks and his group, and for electronic support from L.E. Gibson of R.C. Kaifer's counting group, and from H.R. Buddingh and his maintenance group.

REFERENCES

[1]C.D. Schrader, J. Benveniste, and J.H. Zenger, Gamma Rays from the Interaction of 14-Mev Neutrons Using Time-of-Flight Techniques, Bull. Am. Phys. Soc., Series II, 2, 309 (1957).

[2]W. Weber, C.W. Johnstone, and L. Cranberg, Time-to-Pulse-Height Converter for Measurement of Millimicrosecond Time Intervals, Rev. Sci. Instr. 27, 165 (1956).

[3]J. Benveniste, A.C. Mitchell, C.D. Schrader, and J.H. Zenger, The Problem of Measuring the Absolute Yield of 14-Mev Neutrons by Means of an Alpha Counter, UCRL-5619, June 23, 1959.

[4]Jack Benveniste and Jerry Zenger, Information on the Neutrons Produced in the $He^3(d, n)He^4$ Reaction, UCRL-4266, Jan. 1954.

[5]M.E. Wyman, E.M. Fryer, and M.M. Thorpe, (n, t) Cross Sections for B^{10}, B^{11} and Be^9, Phys. Rev. 112, 1264 (1958).

[6]S.S. Vasil'ev, V.V. Komarov, and A.M. Popova, Effective Cross Section of the $Be^9(n, 2n)$ Reaction, JETP 6, 411 (1958). Translated from Zhur. Eksptl. i Teoret. Fiz. 33, 527 (1957).

[7]This system was conceived and developed by K. Aaland and P.E. Frazier.

[8]The operation of this buncher was originally described by M.P. Nakada in UCRL-4641 (Production of Short Bursts of Neutrons) Sept. 1955.

[9]We are indebted to S. Block for this measurement.

[10]J.M. Blatt and V.F. Weisskopf, Theoretical Nuclear Physics (Wiley, New York, 1952).

[11]I. Bloch et al., Coulomb Functions for Reactions of Protons and Alpha-Particles with Lighter Nuclei, Revs. Modern Phys. 23, 147 (1951).